nature photonics
FOCUS | REVIEW ARTICLES
PUBLISHED ONLINE: 31 OCTOBER 2012 | DOI: 10.1038/NPHOTON.2012.262

# Graphene plasmonics

A. N. Grigorenko[1*], M. Polini[2] and K. S. Novoselov[1]

**Two rich and vibrant fields of investigation—graphene physics and plasmonics—strongly overlap. Not only does graphene possess intrinsic plasmons that are tunable and adjustable, but a combination of graphene with noble-metal nanostructures promises a variety of exciting applications for conventional plasmonics. The versatility of graphene means that graphene-based plasmonics may enable the manufacture of novel optical devices working in different frequency ranges—from terahertz to the visible—with extremely high speed, low driving voltage, low power consumption and compact sizes. Here we review the field emerging at the intersection of graphene physics and plasmonics.**

Graphene, a two-dimensional (2D) form of carbon in which the atoms are arranged in a honeycomb lattice[1,2], has already been shown to possess unique mechanical, electric, magnetic and thermal properties with a multitude of exciting applications that are being vigorously pursued by academia and industry[3]. Interestingly, it is in optics where graphene has shown its 'true colours' and where the first commercial application of graphene has been realized[4]. Graphene has an extremely high quantum efficiency for light–matter interactions, is strongly optically nonlinear and contains plasmons with unusual properties. Furthermore, it can be modified by gating, by doping, by chemical means and through conventional plasmonics based on noble metals. The optics and photonics of graphene have been reviewed several times previously[4–8]. However, the recent proliferation of works on graphene plasmonics and the optics of 2D single-layer materials calls for a fresh look at graphene and its remarkable properties.

## Optical properties of graphene

Among many of the unique properties of graphene[3], probably the most peculiar is the fact that quasiparticles in this material obey a linear dispersion relation. As a result, an additional—chiral—symmetry exists for the quasiparticles, which fixes the direction of pseudospin (in a given valley - a simply connected part of a Fermi surface) to be parallel or antiparallel to the directions of motion of electrons and holes, respectively[9]. This has an immediate, and dominant, effect on the electronic and optical properties of this 2D crystal. One consequence is that the optical conductivity is independent of any material parameters: $\sigma_{\rm uni} = \pi e^2 / (2h)$, where $e$ is electron charge and $h$ is Planck's constant[10,11]. Thus, the optical absorption depends only on the fine-structure constant, $\pi\alpha \approx 2.3\%$ (Fig. 1a). Such simple behaviour is expected for undoped samples at zero temperatures. Doping has a very strong effect on the optical properties[12]: Pauli blocking (Fig. 1b) ensures that photons with energy less than $2E_{\rm F}$ (where $E_{\rm F}$ is the Fermi energy) are not absorbed[13]. Recently, gating with a solid electrolyte allowed carrier concentrations as large as $10^{14}$ cm$^{-2}$ to be achieved, which converts into $E_{\rm F} \approx 1$ eV, such that a modulation of optical transmission in the visible spectrum is possible[12,14,15]. Combining graphene with silicon waveguides, for example, makes it possible to produce a broadband, graphene-based, waveguide-integrated optical modulator[15] (Fig. 1c).

For photon energies greater than 3 eV, trigonal warping effects and deviations from linear dispersion become extremely strong. The band structure of graphene has saddle points at the M points of the Brillouin zone, which lead to van Hove-like singularities. In the single-electron approximation, this should result in a strong absorption peak (of more than 10%) at around 5.2 eV. In practice, this simple picture fails owing to many-body effects, and the peak is observed close to 4.5 eV (refs 16, 17; Fig. 1a).

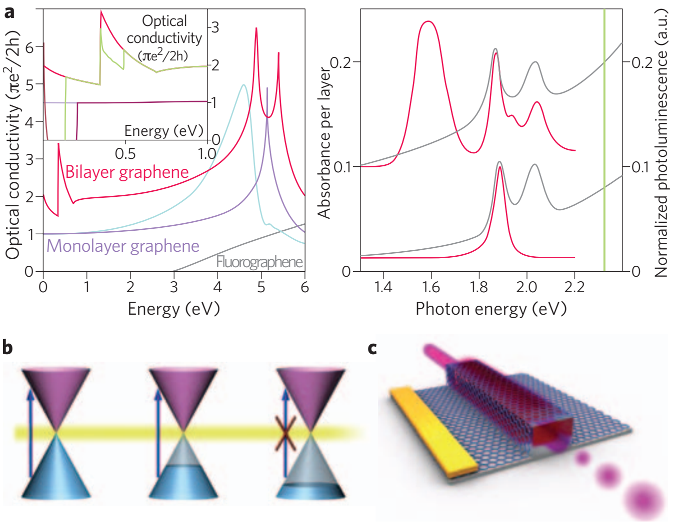

**Figure 1 | Building blocks of 'flatland' optics. a**, Left: the optical conductivities of pristine graphene, with (blue) and without (purple) electron–electron interactions taken into account; pristine bilayer graphene (red); doped graphene (pink); doped bilayer graphene (dark green); and fluorographene (black). The inset shows an enlarged view of the low-energy spectral range. Right: absorption spectra of monolayer and bilayer MoS$_2$ (left axis, normalized by the number of layers; black) and the corresponding photoluminescence spectra (right axis, normalized by the intensity of the peak absorption; red). The spectra are displaced in the vertical axis for clarity. The green line shows the spectral position of the excitation wavelength. a.u., arbitrary units. **b**, Schematic band structure of graphene for various levels of doping (only one valley is shown) and Pauli blocking of photon absorption in graphene. **c**, Sketch of a graphene-based, waveguide-integrated optical modulator, where voltage applied to graphene is used to achieve broadband and high speed modulation of the guided light (adapted from ref. 15). Data in **a** are partly taken from ref. 24.

## Optical properties of other 2D materials

It is often overlooked that the realization that graphene has a number of nontrivial, interesting and possibly useful properties opened a floodgate, resulting in the discovery and study of other 2D crystals

---

[1]School of Physics and Astronomy, University of Manchester, Manchester M13 9PL, UK. [2]NEST, Istituto Nanoscienze-CNR and Scuola Normale Superiore, I-56126 Pisa, Italy. *e-mail: sasha@manchester.ac.uk

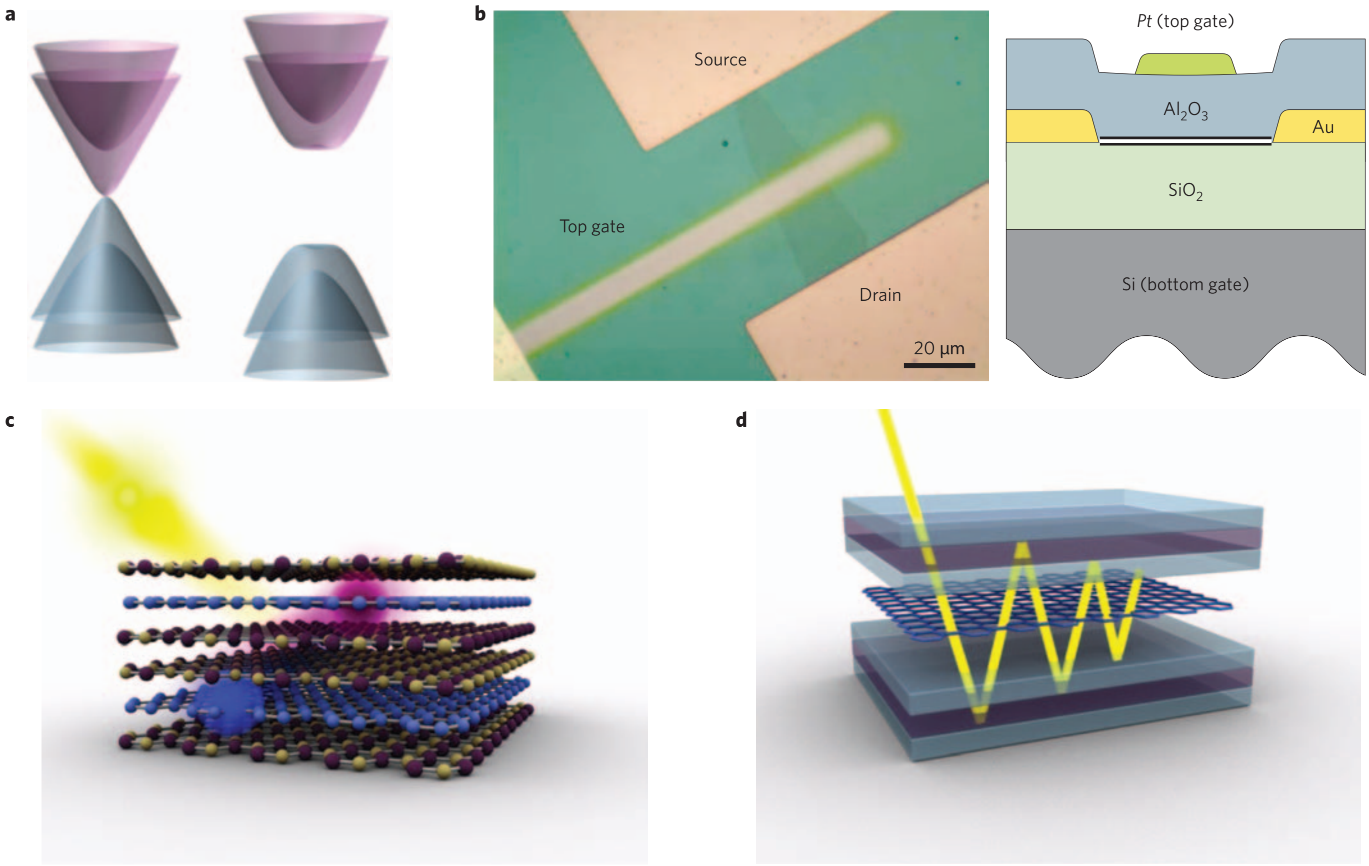

**Figure 2 | Multilayered flatland optics.** **a**, Energy spectra for pristine (left) and doped bilayer (right) graphene , with a gap opening for the latter case. **b**, Optical modulator based on the tunable bandgap in bilayer graphene. **c**, Hypothetical multilayer structure with vertical charge separation. In this particular structure two graphene layers are separated by an optically active barrier. An absorbed photon is converted into an electron-hole pair, which can be split in the external electric field. **d**, Cavity-based graphene photodetector and graphene-based integrated interferometer. By allowing multiple reflections the interaction between light and graphene is strongly enhanced. Images reproduced with permission from ref. 18 (**b**) and ref. 32 (**d**, adapted).

and heterostructures based on them. Over the last few years, many other 2D materials have been intensively investigated. Their optical properties are exciting and often different from the properties of their three-dimensional parent materials.

**Bi- and trilayer graphene: materials with controllable bandgaps and controllable optical absorption.** The electronic structure of bilayer graphene is drastically different from that of the monolayer. The band structure of graphene with A–B (Bernal) stacking is gapless. The valence and conduction bands have parabolic dispersion and touch at zero energy. It also contains additional subbands that, in the first approximation, are offset from zero energy by $\gamma_1 \approx 0.4$ eV (the nearest-neighbour hopping between layers). In optics, this leads to a strong absorption peak at this energy (Fig. 1a).

The gapless spectra in mono- and bilayer graphene are protected by the symmetry between the sublattices. However, in bilayer graphene such symmetry can be easily lifted by selective chemical doping of one of the layers or by applying a transverse electric field (gating). This leads to the opening of a significant gap, which can be seen in optical absorption. Figure 2a shows the energy spectrum of bilayer graphene, and Fig. 2b demonstrates an effective optical modulator based on the tunable bandgap in bilayer graphene[18].

Trilayer graphene is another interesting material, which comes in two very different configurations. The electronic structure of Bernal-stacked (A–B–A) trilayer graphene can be viewed as a combination of those of one monolayer and one bilayer. However, trilayers with rhombohedral (A–B–C) stacking more closely resemble bilayer graphene. As a result, the optical properties of both are strongly dependent on the perpendicular electric field, with the A–B–C trilayer demonstrating a larger bandgap than the A–B–A form.

**Graphane and fluorographene.** Graphene can also be considered a giant aromatic molecule that can undergo chemical reactions. Two such chemically modified forms have already been made: graphane[19] (in which a hydrogen atom is attached to each of the carbon atoms) and fluorographene[20,21] (or 2D Teflon, in which one fluorine atom is attached to each carbon atom). Covalently bonded hydrogen or fluorine changes the hybridization of carbon atoms from $sp^2$ to $sp^3$, which removes the $\pi$ orbitals from the electronic band structure. This should lead to the opening of a large gap of the order of the separation between the $\sigma$ bands. Experimentally, optical gaps of the order of 3 eV have been observed[20] for fluorographene (Fig. 1a).

**2D atomic crystals and their heterostructures.** Monolayer molybdenum disulphide ($MoS_2$) is probably the second most-studied 2D material after graphene. It has been exfoliated to the monolayer state by both mechanical[22] and liquid-phase[23] exfoliation. The properties of monolayer $MoS_2$ are radically different from the properties of the 3D parent material. Bulk crystals have an indirect bandgap of the order of 1.29 eV. In the 2D state, however, $MoS_2$ has a direct bandgap[24] of the order of 1.9 eV around the K points of the Brillouin zone, which leads to a strong increase in luminescence[25] (Fig. 1a).

Furthermore, owing to the absence of inversion symmetry, strong spin–orbit interactions split the valence band states at the K and K′

points by about 0.16 eV. In addition, time reversal symmetry ensures that this splitting is in the opposite direction in the two valleys, leading to opposite spin polarizations in the K and K′ valleys. Effectively, this allows optical control (by means of circularly polarized light) of the population of charge carriers separately in each of the two valleys, leading to the realization of 'valleytronics'[26].

The electronic and optical properties of other 2D crystals (for example BN (ref. 27), $TaS_2$, $NbSe_2$ and $WS_2$) are currently being intensively investigated. It is likely that there will be more surprises from heterostructures created by stacking such 2D crystals one on top of another[28]. The simplest possible stacks have already revealed new physics[29–31], and could revolutionize some applications. The optical properties of these heterostructures can be tuned very accurately, as materials with very different bandgaps and thicknesses can be combined (Fig. 2c). Another direction is to combine graphene heterostructures with standard optics, for example optical cavities[32–34], and optoelectronic devices, for example integrated interferometers[5] (Fig. 2d).

## Intrinsic graphene plasmons

Plasmons are ubiquitous, high-frequency, collective density oscillations of an electron liquid and occur in many metals and semiconductors[35]. The intrinsic graphene plasmons are refreshingly different from plasmons in noble metals as they can be tuned by gating or doping. Graphene plasmonic resonances could have a pivotal role in the realization of robust and cheap photodetectors of terahertz radiation[36], with important security applications. Here we consider the peculiar properties of the intrinsic plasmon modes of the electron gas in a pristine graphene sheet. Our focus is on the plasmons of doped samples, although interesting collective modes have also been predicted for undoped graphene[37]. Moreover, we will focus on longitudinal modes, that is, modes whose associated electric field is parallel to the wave vector, **q**. Such modes are also known as transverse magnetic modes. The existence of a transverse collective mode in graphene (with a frequency slightly lower than the Pauli-blocking threshold for interband absorption) has been also discussed[38]. This mode is also referred to as transverse electric modes. The transverse electric mode in graphene has a frequency, ω, that lies in the window $1.667 < \hbar\omega/E_F < 2$ (where ħ denotes Planck's constant divided by 2π) and can be tuned from the radio-frequency range to the infrared by changing the density of charge carriers using a gate voltage[38]. On the other hand, the transverse magnetic (longitudinal plasmon) mode is gapless in the long-wavelength limit, because its energy vanishes as $q = |\mathbf{q}| \to 0$ (see below).

**Electron plasma in two dimensions.** Two-dimensional electron systems (2DESs) have been a rich source of exciting physics for more than four decades. As in any 2DES, electrons in graphene do not move as independent particles. Rather, their motions are highly correlated as a result of pairwise interactions. These are described by a potential $u(r_{ij}) = u(|\mathbf{r}_i - \mathbf{r}_j|)$, which depends only on the absolute value of the relative distance, $\mathbf{r}_{ij} = \mathbf{r}_i - \mathbf{r}_j$, between two electrons. The interaction potential is sensitive to the dielectric media surrounding the graphene sheet. For graphene with one side exposed to a medium with dielectric constant $\varepsilon_1$ and the other exposed to one with dielectric constant $\varepsilon_2$, we have $u(r_{ij}) = e^2/\varepsilon r_{ij}$, where $\varepsilon = (\varepsilon_1 + \varepsilon_2)/2$ (such that the 2D Fourier transform is $u_q = 2\pi e^2/\varepsilon q$). The electron gas in a graphene sheet can be described at low energies by the following continuum-model Hamiltonian:

$$\hat{H} = v_F \sum_i \boldsymbol{\sigma} \cdot \mathbf{p}_i + \frac{1}{2} \sum_{i \neq j} \frac{e^2}{\varepsilon |\mathbf{r}_i - \mathbf{r}_j|}, \qquad (1)$$

Here $v_F \approx 10^6$ m s$^{-1}$ is the Fermi velocity, $\mathbf{p}_i = -i\hbar\nabla_{\mathbf{r}_i}$ is the canonical momentum of the $i$th electron and $\boldsymbol{\sigma} = (\sigma_x, \sigma_y)$ is a 2D vector of the Pauli matrices. For the sake of simplicity, equation (1) has been written for a single-channel, massless Dirac fermion (MDF) model; that is, it holds for electrons with given spin and valley indices. The relative importance of electron–electron interactions is quantified by the ratio between the 'magnitude' of the second term and that of the first term. For a doped graphene sheet, the typical distance between electrons is of the order of the inverse of the Fermi wavenumber, that is, $k_F^{-1}$. The second term is thus of the order of $e^2 k_F/\varepsilon$. The kinetic energy is of the order of $\hbar v_F k_F$ and, hence, the ratio between these two quantities defines a dimensionless parameter, $\alpha_{ee}$, usually called the graphene fine-structure constant:

$$\alpha_{ee} = \frac{e^2}{\varepsilon \hbar v_F}$$

This can be expressed using the conventional fine-structure constant, $\alpha = e^2/\hbar c$, as $\alpha_{ee} = c\alpha/\varepsilon v_F$, which allows us quickly to estimate the magnitude of $\alpha_{ee}$. For example, for graphene with one side exposed to air ($\varepsilon_1 = 1$) and the other to $SiO_2$ ($\varepsilon_2 \approx 3.9$), we have $\alpha_{ee} \approx 0.9$. For a suspended graphene sheet, $\varepsilon_1 = \varepsilon_2 = 1$ and $\alpha_{ee} \approx 2.2$. Hence, the graphene fine-structure constant can be tuned experimentally by changing the dielectric environment surrounding graphene[39]. From this analysis, we conclude that, at least in principle, electrons in a doped graphene sheet interact quite strongly with each other and that interaction effects in this material have to be analysed with great care.

**Theory of 2D plasmons.** The physical origin of plasmons can be understood as follows. When electrons move to screen an electric field, they tend to travel slightly too far (Fig. 3a). They are then pulled back toward the charge disturbance and overshoot again, setting up a weakly damped oscillation. The restoring force responsible for the oscillation is proportional to the gradient of the self-consistent field created by all the electrons. The plasmon dispersion in a 2DES can be understood in the long-wavelength, $q << k_F$, limit on the basis of hydrodynamics. In this limit, a macroscopic description for the electron dynamics can be used by defining two collective variables[35] that obey macroscopic conservation laws: the deviation of the electron density from its average value, $\delta n(\mathbf{r}, t)$, and the associated current density, $\delta\mathbf{j}(\mathbf{r}, t)$. For $|\delta n/n| << 1$ (where $|n|$ is the average carrier density of the doped sheet), the plasmons are described by the following linearized Euler equation of motion:

$$\frac{\partial \mathbf{j}(\mathbf{r},t)}{\partial t} = -\frac{D}{\pi e^2} \nabla_r \int d^2\mathbf{r}' \frac{e^2}{\varepsilon |\mathbf{r} - \mathbf{r}'|} \delta n(\mathbf{r}',t)$$

In conjunction with the continuity equation, this leads to the following equation for the Fourier component of $\delta n(\mathbf{r}, t)$, where $D$ is the Drude weight:

$$\left[\omega^2 - \frac{D}{\pi e^2} q^2 u_q\right] \delta n(\mathbf{q},\omega) = 0 \qquad (2)$$

Equation (2) implies the existence of plasmons with a frequency $\omega_{pl}(q) = \sqrt{2Dq/\varepsilon}$. We note that $\omega_{pl}(q) \propto \sqrt{q}$, which is a peculiarity of plasmon oscillations in two dimensions. For ordinary Schrödinger fermions with mass $m_b$, the Drude weight is given by $D = \pi e^2 n/m_b$ and we have the well-known result $\omega_{pl}(q) = \sqrt{2\pi n e^2 q/(\varepsilon m_b)}$. The situation turns out to be quite different for MDFs in graphene. The Drude weight of (non-interacting) MDFs is given by $D_{MDF} = 4E_F\sigma_{uni}/\hbar$, which yields the following plasmon frequency in doped graphene[40–43] in the long-wavelength limit:

$$\omega_{pl}(q) = \sqrt{\frac{8E_F\sigma_{uni}\,q}{\hbar\varepsilon}} \qquad (3)$$

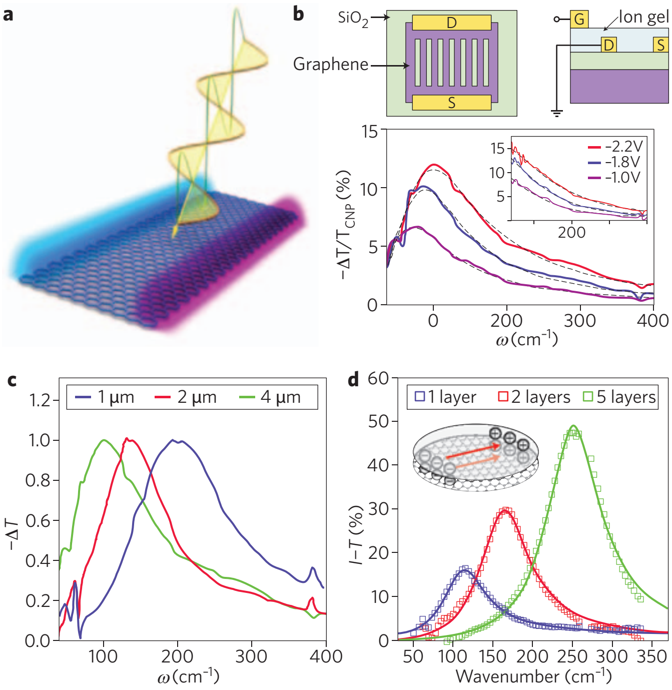

**Figure 3 | Intrinsic graphene plasmons. a**, The schematics of plasmon excitation. **b**, Plasmon resonance in gated graphene microribbon arrays. Top: top and side views of a typical graphene microribbon array. D, drain; G, gate; S, source Bottom: gate-induced change of relative transmission spectra, as a function of excitation frequency for three different gate voltages. **c**, Control of plasmon resonance through microribbon width. Transmission spectra for the samples of different widths and the same doping concentration. **d**, Transparent graphene plasmonic devices. Extinction in stacked plasmonic devices with one, two and five graphene layers. Figures reproduced with permission from ref. 56 (**b** and **c**) and ref. 58 (**d**).

The Dirac plasmon frequency thus scales like $E_F^{1/2} \propto n^{1/4}$ and contains Planck's constant. When the plasmon energy becomes larger than the threshold for interband transitions, plasmons become strongly Landau damped. For a typical doping, $n = 10^{11}$ cm$^{-2}$, the Fermi energy in graphene is $E_F \approx 37$ meV and the plasmon energy for graphene on SiO$_2$ at $q = 0.1k_F \approx 0.6 \times 10^5$ cm$^{-1}$ is about 16 meV, which is in the infrared range. One remarkable conclusion of equation (3) is that the compression of the surface plasmon wavelength relative to the excitation wavelength is governed by the fine-structure constant and can be strong[6] because $\lambda_{pl}/\lambda_0 \approx 2\alpha E_F/(\varepsilon\hbar\omega) \sim \alpha$.

When $q \approx k_F$, the hydrodynamic approach described above is not adequate to describe the plasmon dispersion relation quantitatively. The key ingredient of a fully quantum mechanical calculation of plasmon modes is the retarded density–density response function[35], $\chi_{nn}(q,\omega)$, which, in the framework of linear response theory and within the random phase approximation (RPA), is given by $\chi_{nn}^{RPA}(q,\omega) = \chi_{nn}^{(0)}(q,\omega) / \varepsilon(q,\omega)$, where $\chi_{nn}^{(0)}(q,\omega)$ is the well-known[40,41,44,45] non-interacting response function and $\varepsilon(q, \omega)$ is the RPA dynamical dielectric function. The function $\chi_{nn}^{(0)}(q,\omega)$is usually referred to as the 'Lindhard function'. The RPA is not exact, but it is typically a good starting point for ordinary Fermi liquids (see, however, the discussion in ref. 46). Higher-order terms in the dispersion relation in equation (3) in an expansion in powers of $q/k_F$ are given in ref. 47.

So far, we have discussed plasmons in doped graphene sheets at zero temperature and in the absence of disorder. The effects of finite temperature and disorder can be incorporated in the RPA theory by using the appropriate Lindhard function at finite temperature[48] and the Mermin approximation[49], respectively. It is worth noting that plasmon losses in graphene are expected to be considerably smaller than those in normal metals. The plasmon lifetime, $\tau_{pl}$, however, should not be confused with the d.c. transport scattering time, $\tau_{tr}$. (This confusion often arises in quantitative analyses of plasmonic effects in graphene: in this context, the simple Drude formula for the frequency-dependent conductivity, $\sigma(\omega)$, which depends only on $\tau_{tr}$, is typically used[6,49,50].) For massive 2D electrons, it has been shown[51] that $\tau_{pl} \approx \tau_{tr}$ in the high-density regime but that in the low-density regime $\tau_{pl}$ can be much smaller than $\tau_{tr}$. In addition, plasmons could decay in the absence of disorder, by emitting, for example, two electron–hole pairs with opposite momenta[35]. This many-body effect is not captured by the RPA. To the best of our knowledge, all these issues have yet to be investigated and much more theoretical and experimental work is needed to understand and quantify plasmon losses in graphene and other 2D crystals.

**The effect on Dirac plasmons of screening due to a metal gate.** Here we briefly discuss the effect that screening by a metal gate has on the Dirac plasmon dispersion (equation (3)) in a doped graphene sheet. Neglecting effects of hybridization between graphene and metal, we can describe a metal as a grounded conductor screening the Coulomb interactions between electrons in graphene. This formally leads to the replacement $u_q \rightarrow U_d(q) = 2\pi e^2(1 - e^{-2qd})/q$, where $d$ is the distance between the graphene and the gate. Because $U_d(q)$ is regular at $q = 0$, we expect a gapless acoustic plasmon with $\Omega_{ac}(q \rightarrow 0) = c_s q$ rather than an 'unscreened plasmon' (equation (3)) with $\omega_{pl}(q) \propto \sqrt{q}$. An RPA expression for $c_s$ is derived in ref. 52.

**Experimental observations of intrinsic plasmons in graphene.** Plasmons in 2DESs can be accessed by a variety of direct and indirect methods, including optical measurements, electron energy-loss spectroscopy, inelastic light scattering, angle-resolved photoemission spectroscopy (ARPES) and scanning tunnelling spectroscopy. Several experiments on electron energy-loss spectroscopy have been performed on exfoliated graphene sheets[53] and on epitaxial graphene samples[54], which showed that Dirac plasmons in graphene on SiC are strongly hybridized with the surface optical phonons of the SiC substrate[55]. Dirac plasmons have also been probed by directly engineering their coupling to infrared light in a number of intriguing ways[50,56–60].

The study of large-area arrays of graphene microribbons grown by chemical vapour deposition has shown that infrared light polarized perpendicular to the ribbon axis is able to excite plasmon resonances of the confined MDF gas[56] (Fig. 3b). In these experiments an ion gel was used for gating, yielding an induced carrier concentration of about $10^{13}$ cm$^{-2}$, which allowed the authors to access the terahertz spectral range. Plasmon excitations in graphene microribbon arrays can be varied by electrical gating[58] (Fig. 3b). Furthermore, the plasmon frequency scales like $W^{-1/2}$, where $W$ is the width of the ribbon, and like $n^{1/4}$, in agreement with the bulk RPA prediction in equation (3) (Fig. 3c). Graphene-microribbon-based plasmonic waveguides 6 mm long allowed the transmission of 2.5 Gbps optical signals with an average extinction ratio of 19 dB at a wavelength of 1.31 μm (ref. 60). Recently, plasmon hybridization in coupled graphene nanoribbons has been demonstrated[61] and splitting of plasmons in graphene nanostructures into bulk and edge modes in high magnetic fields has been observed[62].

The direct interaction of localized graphene plasmons with infrared light has been demonstrated[58] (Fig. 3d) using a stack of graphene microdiscs, which allowed the plasmons to be tuned through changing the disk diameter, the number of discs, the filling number and the gating (Fig. 3d). It was found that the collective oscillation of

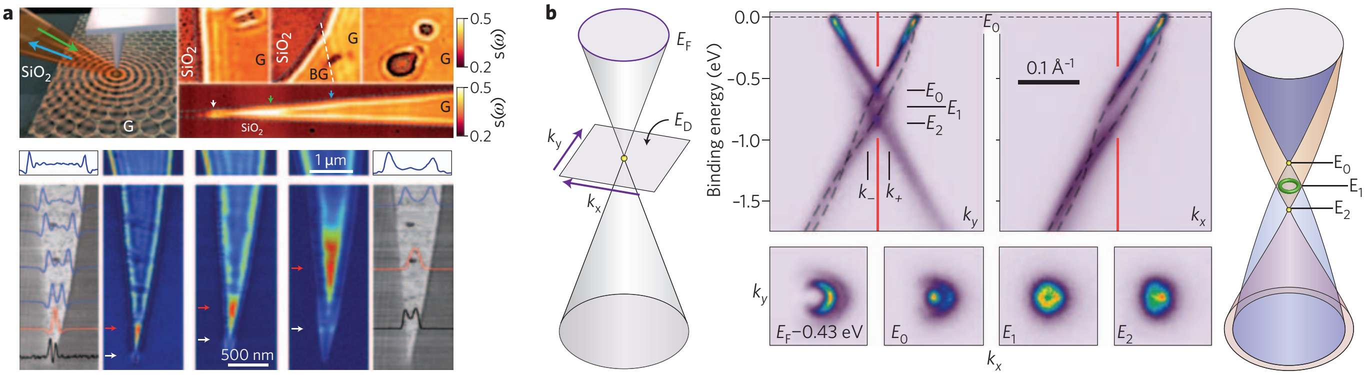

**Figure 4 | Launching and imaging graphene plasmons. a**, Top left: schematic of an infrared nano-imaging experiment. The blue and green arrows label the incoming and back-scattered light, respectively. Top right: images of various interference patterns close to graphene edges (blue dashed lines), defects (green dashed lines), or boundaries between monolayer (G) and bilayer (BG) graphene (white dashed line). Scale bar represents normalized near-field amplitude of excited plasmons. Arrows show features connected to plasmon interference. Bottom: controlling the plasmon wavelength in scattering experiments. The control is based on strong dependence of graphene plasmons on dielectric properties of substrate. From left to right the excitation wavelength changed from 9,200nm to 10,152nm, the permittivity of substrate from 2.9 to 0.7, and the plasmon wavelength from 200nm to 700nm. **b**, Plasmaron satellite bands in the ARPES spectrum of graphene on SiC. Left: The Dirac energy spectrum of graphene in a non-interacting picture as a function of the two components of momentum, $k_x$ and $k_y$. $E_D$ indicates the energy of the "Dirac point", where the upper and lower Dirac cones touch. $E_0$, $E_1$ and $E_2$ are the characteristic energies of the reconstructed Dirac crossing. Middle-top panel: Experimental spectrum of doped graphene perpendicular and parallel to the Γ–K direction. The dashed lines are guides to the dispersion of the observed hole and plasmaron bands. The red lines are at $k = 0$. Middle-bottom panels: Constant-energy cuts of the spectral function at different binding energies. Right panel: Schematic Dirac spectrum in the presence of electron–electron interactions. Figures reproduced with permission from refs 50, 59 (**a**) and ref. 66 (**b**).

MDFs is unambiguously quantum mechanical, with the $n^{1/4}$ scaling of the plasmon frequency. In addition, it was shown how stacked graphene microdiscs could be used as an electromagnetic radiation shield with 97.5% effectiveness, a tunable, far-infrared notch filter with a rejection ratio of 8.2 dB and a tunable, terahertz linear polarizer with an extinction ratio of 9.5 dB (ref. 58).

Perhaps the most striking were the recent observations of intrinsic graphene plasmons in refs 50, 59, where the authors used the tip of an atomic force microscopy (AFM) probe in a scattering-type scanning near-field optical microscopy set-up to launch and image Dirac plasmons in real space. A schematic picture of the experiments carried out and some of the findings are summarized in Fig. 4A. Infrared nano-imaging revealed that the plasmon wavelength compression ratio, $\lambda_0/\lambda_{pl}$, can reach 40 and that the plasmon in confined geometries can be tuned by gating. The strong confinement of graphene plasmons made it possible to use a single-molecule defect in graphene as an atomic antenna in the petahertz frequency range[63].

Nanoscale morphological defects, such as atomic steps and wrinkles, in epitaxial graphene on SiC are responsible for a strong terahertz plasmonic peak in the optical response[64]. Plasmons in epitaxial graphene can thus couple to terahertz light in the absence of artificial lithographic patterning. To summarize, so far experiments have confirmed the long-wavelength ($q << k_F$) 2D plasmon dispersion law, $\omega_{pl}(q) \propto \sqrt{q}$ ; the $n^{1/4}$ scaling of the plasmon frequency (the dependence on average density, $n$, has been checked in the same sample by means of electrostatic gating, demonstrating that plasmons in graphene are gate-tunable); and the giant confinement of light into small volumes.

The possibility of changing the plasmon frequency easily by using gates is important. However, Dirac plasmons are noteworthy for other reasons: the Dirac plasmon dispersion suffers renormalizations due to exchange and correlation effects even in the long-wavelength limit[43]; Dirac plasmons can be manipulated using surface-science techniques; it is easy to couple Dirac plasmons to light provided that the momentum mismatch between the two is compensated by a sufficiently 'sharp' object (for example a periodic pattern, the tip of an AFM probe or a nanoscale defect); and the lifetime of Dirac plasmons is expected to be much longer than that of plasmons in metals or semiconductors.

**Plasmarons.** Condensed matter physics is rich in examples of 'composite' quasiparticles, which are often bound states of bare electrons or holes with collective excitations of a many-particle medium, for example surface plasmon polaritons. Composite quasiparticles formed by the coupling of elementary charges to plasmons are called plasmarons. Their existence has been predicted[42,65] and then demonstrated[66,67] in doped graphene sheets. A plasmaron can be regarded as a 'dressed' electron (or a hole) interacting with plasmonic vibrations[68]. Plasmarons can be observed by optical and tunnelling spectroscopy. Recently, a series of high-resolution ARPES experiments on high-quality graphene sheets grown on SiC was used to demonstrate a massive reconstruction of the MDF chiral spectrum near the Dirac point of doped samples[66,67]. A representative set of ARPES data for the spectral function of the electron gas in a quasi-freestanding graphene sheet is shown in Fig. 4B.

**Plasmon–electron interactions in graphene.** The particle–hole continuum of a non-interacting gas of MDFs is represented by the imaginary part of the Lindhard function, which (for an undoped system and positive frequency $\omega$) is given by

$$\mathrm{Im}[\chi^{(0)}_{nn}(q,\omega)]\,|_{undoped} = -\frac{q^2}{4\hbar}\frac{\Theta(\omega - v_F q)}{\sqrt{\omega^2 - v_F^2 q^2}}$$

The main feature here is the divergence of $|\omega^2 - v_F^2q^2|^{-1/2}$ that occurs near the 'light cone', $\omega = v_Fq$: this arises because of collinear scattering processes among MDFs. For finite doping, a triangular region is removed from the particle–hole continuum for small $q$ and $\omega$ owing to Pauli blocking. The spectral density of particle–hole pairs is relatively weak at the lower limit of the $q < k_F$ interband continuum. The plasmon excitation of the Dirac sea emerges in this triangular region of Pauli-blocked particle–hole pairs and remains remarkably well defined even when it enters the interband

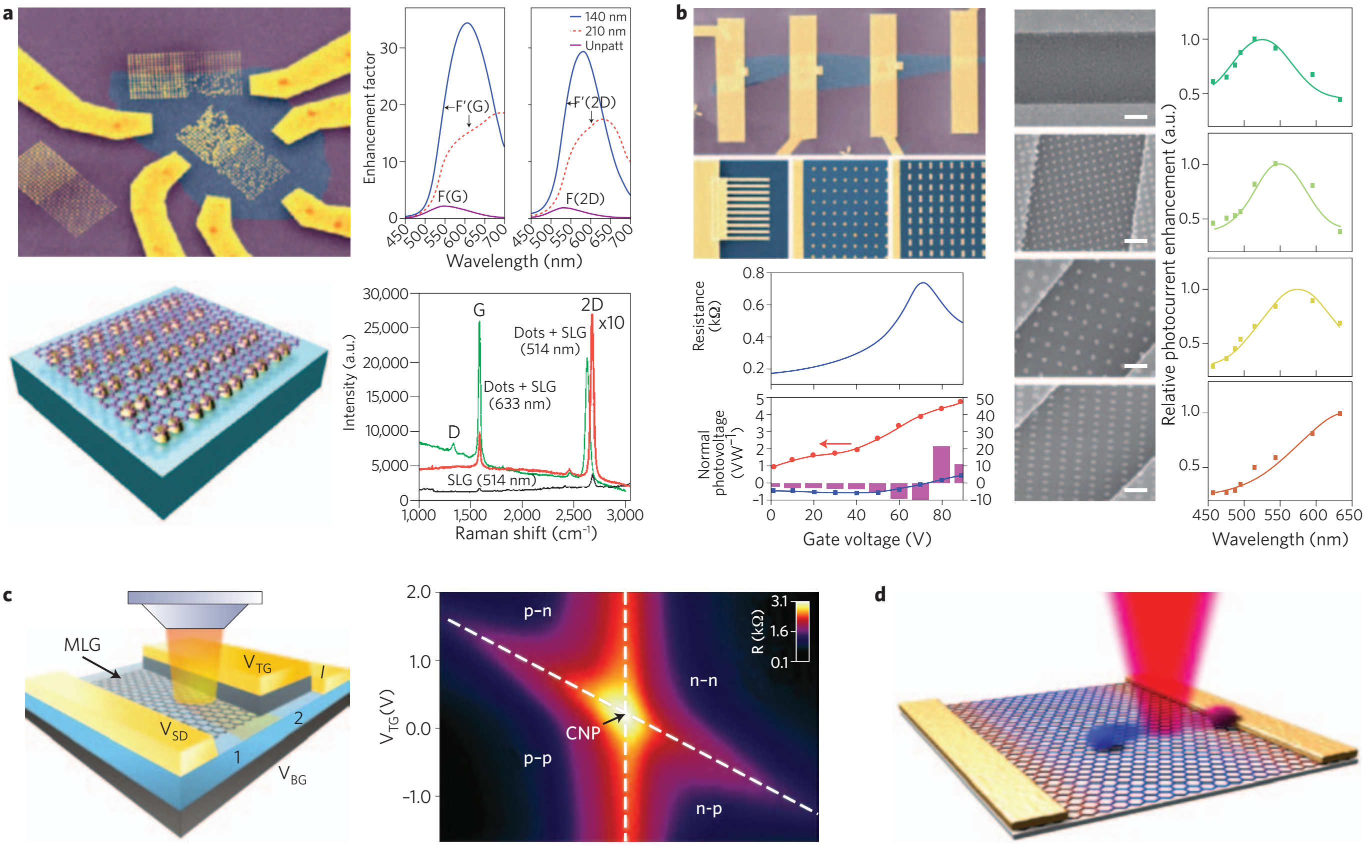

**Figure 5 | Hybrid graphene plasmonic devices. a**, Top left: SEM images of a sample for surface-enhanced Raman spectroscopy. Top right: the total (patterned) enhancement factors F' for the G and 2D Raman peaks for the structures with particle diameter of 140 nm and 210 nm. The black dotted line is the corresponding interference (unpatterned) enhancement factor F. Bottom left: schematics of plasmonic metamaterial (coupled golden nanodots on a glass substrate in this particular case) and graphene. Bottom right: Raman spectra of single-layer graphene (SLG) placed on top of gold nanodots, measured at 514 and 633 nm. **b**, Top left: SEM images of graphene photodetectors with plasmonic nanostructures. L, θ and TR represent the state of light polarization. Top right: the corresponding resistance and photovoltaic characteristics for devices with (red squares) and without (blue) plasmonic nanostructures. Solid bars indicate the enhancement ratio (right-hand scale). Bottom: multicolour photodetection using graphene devices coupled to plasmonic nanostructures (left, SEM images; right, corresponding photoresponses). **c**, Device geometry and optoelectronic characteristics of the graphene p–n junction. Left: experimental schematics. Here $V_{BG}$, $V_{TG}$ and $V_{SD}$ are the voltages of the back, top and side gates, respectively. Right: resistance versus $V_{BG}$ and $V_{TG}$ at $V_{SD} = 1.4$ mV and $T = 175$ K. (CNP stands for charge neutrality point). **d**, Schematics of charge separation for graphene doped by metallic contacts Built-in electric field (created at the metal-graphene interface due to the difference in the work functions) separates electron-hole pairs, thus creating photocurrent. Figures reproduced with permission from refs 75, 76 (**a**), refs 81, 82 (**b**) and ref. 86 (**c**).

continuum: interactions between quasiparticles and plasmons are stronger[42] in 2D MDFs than in an ordinary non-relativistic 2DESs.

In a doped graphene sheet, it is necessary to take dynamical screening into account, which is typically accomplished by considering the RPA effective interaction, $W(q, \omega) = u_q/\varepsilon(q, \omega)$. Calculating the 'self-energy' of quasiparticles within the RPA shows that at some specific wavenumber, the bare quasiparticle velocity equals the plasmon group velocity. In the case of doped graphene, a charge carrier scatters into a resonance consisting of a quasiparticle 'travelling together' with (that is, strongly coupled to) an undamped plasmon excitation, or plasmaron[67,68]. Plasmaron features can also be observed by tunnelling spectroscopy[69,70]. More details on the properties of electron–electron interactions and their influence on graphene optics can be found in other reviews[71,72].

## Graphene-based plasmonics—hybrid devices

Graphene is a versatile, broadband, adjustable and tunable optical material. However, direct applications of graphene in optics and photonics suffer from graphene's relatively inefficient interaction with light. Although it might be argued that 2.3% of absorption of light by a single atomic layer is actually a large number, to achieve effective optical modulators and photocells it is necessary to enhance light–matter interactions in graphene. The combination of graphene with conventional plasmonics based on noble metals[73,74] could, therefore, be beneficial for both fields of investigation: plasmonic nanostructures can enhance the optical properties of graphene (stronger Raman signature, more effective graphene plasmonic photocells and so on), and graphene could be applied to influence the optical response of plasmonic nanoarrays (for optical modulators and sensing) leading to graphene-based active plasmonics.

**Raman scattering in graphene enhanced by near-fields of plasmonic nanostructures.** Metallic nanostructures excited by light often demonstrate localized surface plasmon resonances, which are characterized by strongly enhanced near-fields produced by charges stopping at the surface of the metal. Because interaction of light with graphene is determined by the local electromagnetic fields (induced on the graphene sheet), this interaction can effectively be increased by placing metal nanostructures close to the graphene. This approach was

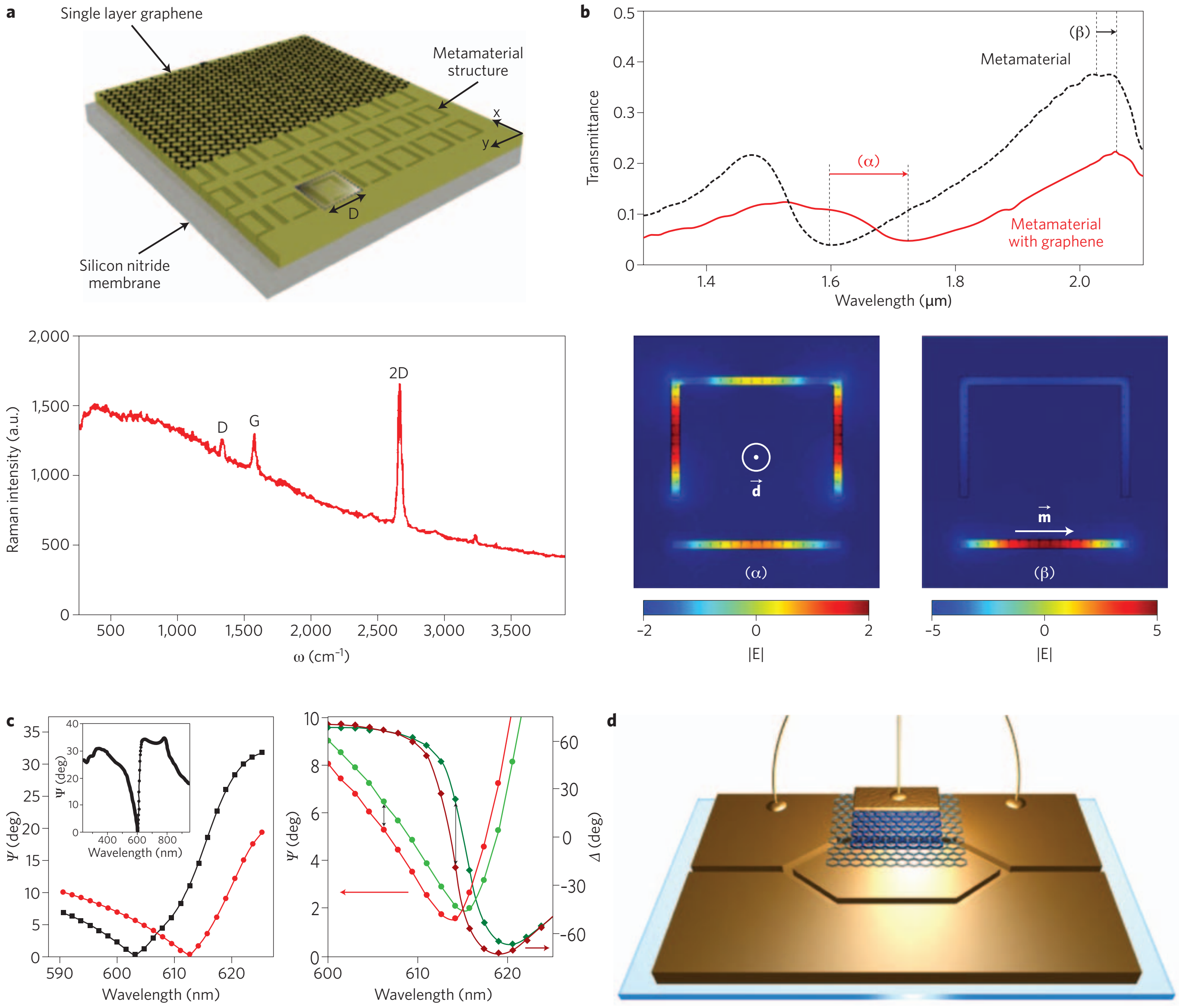

**Figure 6 | Hybrid graphene plasmonic devices. a**, Top: schematic of the fabricated complementary split-ring metamaterial. *D*, is the unit-cell size. Bottom: Raman spectrum corresponding to the marked region. **b**, Top: experimental transmission spectrum of an array before (dashed black line) and after (red solid line) deposition of graphene, for *D* = 711 nm. Bottom: electric field maps at the plasmon resonances. Vectors $\vec{d}$ and $\vec{m}$ represent dipole and magnetic moments respectively. **c**, Evaluation of sensitivity for singular-phase plasmonic detectors. Left: ellipsometric spectra in the region of the collective plasmon resonance for the pristine double-dot array (black curve) and for the array with graphene transferred on top (red curve). Inset, entire spectrum for the pristine case. Right: Ellipsometric parameters $\Psi$ and $\Delta$ for the case of 1% hydrogenated, green curves, and pristine graphene, red curves, as functions of wavelength (incidence angle of 70°). One-sided graphene hydrogenation by 1% corresponds to a change in areal mass density of ~1 pg mm$^{-2}$.
**d**, Hypothetical graphene-based active plasmonic interferometer, with one of the branches covered with graphene on boron nitride, thus allowing for modulation of optical signals. Figures reproduced with permission from ref. 91 (**a**, **b**) and ref. 94 (**c**).

taken in refs 75–78, where the localized surface plasmon resonances of metallic nanodots were used to increase significantly the Raman intensity (Fig. 5a). Graphene provides the ideal prototype test material for investigation of surface-enhanced Raman spectroscopy[79]. Its Raman spectrum is well known[80], and graphene samples are entirely reproducible and can be made virtually defect free. The 2D nature of graphene allows a closed-form description of the Raman enhancement based on the electromagnetic mechanism[74], in agreement with experiments[75]. The development of a generic procedure for graphene transfer on top of a prefabricated plasmonic nanostructure[76] paves the way for the use of graphene as the platform of choice for studying and quantifying field amplification in conventional plasmonics.

**Plasmonic enhancement of photovoltage in graphene.** Near-field enhancement by plasmonic nanostructures was used to improve the efficiency of photovoltage conversion significantly in graphene[81] and to achieve a spectral selectivity that enables multicolour photodetection[82] (Fig. 5b). Graphene-based photodetectors have excellent characteristics in terms of quantum efficiency and reaction time[83], because of the very large room-temperature mobility and high Fermi velocity of graphene's charge carriers. A combination of graphene with plasmonic nanostructures makes it possible to enhance the photovoltage by a factor of 15–20 without compromising the operational speed of a graphene photodetector. It is worth noting that the exact mechanism for light-to-current conversion is still debated[84,85]. Recently, the importance of thermoelectric effects was highlighted in direct measurements[86] of the six-fold symmetry of photovoltage patterns as functions of bottom- and top-gate voltages (Fig. 5c). These patterns, together with the measured spatial and density dependences of the photoresponse, provide evidence that at low temperatures nonlocal hot carrier transport dominates the intrinsic photoresponse in plain graphene with non-structured electrodes[86].

Important building blocks of graphene-based photodetectors are p–n junctions, which are usually required to separate the photo-generated electron–hole pairs. Such p–n junctions are often created close to the contacts, because of the difference in the work functions of metal and graphene[87,88]. The geometrical position (and 'strength') of the p–n junction can be varied by gating, which in turn can be used to modulate the photoresponse of graphene (Fig. 5d). The presence of electric contact between the graphene and the plasmonic nanostructures is important because it could result in resistive coupling of local surface plasmon resonances[89] and lead to additional doping of the graphene sheet. In this respect, vertical geometries such as those shown in Fig. 2c are more beneficial for light harvesting[90].

**Graphene-based plasmonics for modulation and sensing.** The tunability of graphene afforded by gating is vital for the field of active plasmonics. Active optical elements are of great importance in different areas of science and technology, with applications ranging from displays to high-tech frequency modulators. Despite a great deal of progress in optical disciplines, active optics still relies heavily on liquid crystals, which guarantee deep modulation in inexpensive, small cells but are quite slow, and nonlinear optical crystals, which are fast but quite bulky and expensive. For this reason, the development of inexpensive, fast and small active optical elements would be of considerable interest.

Recently, plasmonic metamaterials have established themselves as a versatile tool for creating new optical devices. Their optical properties can be easily controlled by changing the electric coupling between the plasmonic nanoresonators that constitute a nanomaterial. The extraordinary optical, electrical and mechanical properties of graphene can be used to achieve such control. The combination of graphene with plasmonics could result in fast, relatively cheap and small active optical elements and nanodevices. There are two main challenges to this: combining graphene with plasmonic elements and achieving effective control over graphene's properties and the optical response of hybrid optical devices.

In ref. 91, a low-pressure chemical vapour deposition process was used to grow graphene[92] on polycrystalline Cu foils and a poly(methyl methacrylate) wet transfer procedure was then used to transfer graphene on top of prefabricated plasmonic metamaterials (Fig. 6a). The graphene changed the spectral position of the plasmonic resonances of the metamaterial as well as the absolute value of spectral transmission (Fig. 6b). Simple finite-difference time domain calculations[93] provided general support for the experimental data, although the details of graphene resistive coupling to plasmons and graphene doping by the metal are still lacking.

Mechanically exfoliated graphene and a poly(methyl methacrylate) wet transfer procedure have been used to place graphene on top of regular plasmonic nanoarrays[76,94]. These plasmonic nanoarrays possess ultranarrow diffractive-coupled plasmon resonances[95] (or geometric resonances), which show extremely high phase sensitivity to the external environment[96]. The presence of graphene strongly influenced the position of coupled resonances and other optical properties of the samples (Fig. 6). To modify the graphene properties, reversible graphene hydrogenation was performed in which an areal mass sensitivity limit of 0.1 fg mm$^{-2}$ was recorded[94]. This is four orders of magnitude better than the areal sensitivity of the surface plasmon resonance technique[97] and thus opens up the possibility of realizing single-molecule label-free detection. Owing to the well-defined 2D geometry and the possibility of monitoring the hydrogenation level using Raman spectroscopy[98], graphene could become the platform of choice for measuring areal mass sensitivity in plasmonic nanosensors.

The ultimate goal for hybrid graphene–plasmonic elements is to achieve light modulation using graphene gating; see Fig. 6d, where a hypothetical plasmonic interferometer[99] governed by graphene is shown. The presence of metallic nanostructures makes the problem of gating quite complicated owing to electrostatics and electric discharge. The problem of graphene gating in hybrid plasmonic nanodevices is currently under intense investigation.

## Perspective

Graphene, its derivatives and other atomic-monolayer materials could become the building blocks of new generations of multilayer optical devices. The range of building blocks now includes all kinds of optical materials: dielectrics, semiconductors, semimetals, metals, those that are gapless, those that have small and large optical gaps, and so on. We hope that their combination will result in new optical applications (efficient photocells, ultrafast optical modulators and graphene-based 2D lasers) in the near future. The potential of graphene plasmons is also being realized, and they show very attractive features including extremely high localization, strong confinement, efficient and strong light–matter interactions, relatively long lifetimes, tunability and electrical controllability. Light manipulation with intrinsic graphene plasmons and the accessibility of quantum optical regimes promise a revolution in optoelectronics and optical computing. A combination of graphene with conventional plasmonic nanostructures and metamaterials will provide ultrasensitive chemical sensors and biosensors, new nonlinear optical elements and effective photodetectors. We foresee graphene becoming the platform of choice for quantifying field amplification in, and measuring areal sensitivity of, plasmonic devices. Furthermore, the diverse properties of graphene quasiparticles and their interaction with plasmonic vibrations promise new discoveries in fundamental physics.

## References

1. Novoselov, K. S. *et al.* Electric field effect in atomically thin carbon films. *Science* **306,** 666–669 (2004).
2. Novoselov, K. S. *et al.* Two-dimensional gas of massless Dirac fermions in graphene. *Nature* **438,** 197–200 (2005).
3. Geim, A. K. & Novoselov, K. S. The rise of graphene. *Nature Mater.* **6,** 183–191 (2007).
4. Bonaccorso, F., Sun, Z., Hasan, T. & Ferrari, A. C. Graphene photonics and optoelectronics. *Nature Photon.* **4,** 611–622 (2010).
5. Vakil, A. & Engheta, N. Transformation optics using graphene. *Science* **332,** 1291–1294 (2011).
6. Koppens, F. H. L., Chang, D. E. & Javier Garcia de Abajo, F. Graphene plasmonics: a platform for strong light-matter interactions. *Nano Lett.* **11,** 3370–3377 (2011).
7. Tassin, P., Koschny, T., Kafesaki, M. & Soukoulis, C. M. A comparison of graphene, superconductors and metals as conductors for metamaterials and plasmonics. *Nature Photon.* **6,** 259–264 (2012).
8. Bao, Q. & Loh, K. P. Graphene photonics, plasmonics, and broadband optoelectronic devices. *ACS Nano* **6,** 3677–3694 (2012).
9. Castro Neto, A. H., Guinea, F., Peres, N. M. R., Novoselov, K. S. & Geim, A. K. The electronic properties of graphene. *Rev. Mod. Phys.* **81,** 109–162 (2009).
10. Kuzmenko, A. B., van Heumen, E., Carbone, F. & van der Marel, D. Universal optical conductance of graphite. *Phys. Rev. Lett.* **100,** 117401 (2008).
11. Nair, R. R. *et al.* Fine structure constant defines visual transparency of graphene. *Science* **320,** 1308 (2008).
12. Li, Z. Q. *et al.* Dirac charge dynamics in graphene by infrared spectroscopy. *Nature Phys.* **4,** 532–535 (2008).
13. Bao, Q. L. *et al.* Atomic-layer graphene as a saturable absorber for ultrafast pulsed lasers. *Adv. Funct. Mater.* **19,** 3077–3083 (2009).

14. Wang, F. *et al.* Gate-variable optical transitions in graphene. *Science* **320,** 206–209 (2008).
15. Liu, M. *et al.* A graphene-based broadband optical modulator. *Nature* **474,** 64–67 (2011).
16. Kravets, V. G. *et al.* Spectroscopic ellipsometry of graphene and an exciton-shifted van Hove peak in absorption. *Phys. Rev. B* **81,** 155413 (2010).
17. Yang, L., Deslippe, J., Park, C. H., Cohen, M. L. & Louie, S. G. Excitonic effects on the optical response of graphene and bilayer graphene. *Phys. Rev. Lett.* **103,** 186802 (2009).
18. Zhang, Y. B. *et al.* Direct observation of a widely tunable bandgap in bilayer graphene. *Nature* **459,** 820–823 (2009).
19. Elias, D. C. *et al.* Control of graphene's properties by reversible hydrogenation: evidence for graphane. *Science* **323,** 610–613 (2009).
20. Nair, R. R. *et al.* Fluorographene: a two-dimensional counterpart of Teflon. *Small* **6,** 2877–2884 (2010).
21. Robinson, J. T. *et al.* Properties of fluorinated graphene films. *Nano Lett.* **10,** 3001–3005 (2010).
22. Novoselov, K. S. *et al.* Two-dimensional atomic crystals. *Proc. Natl Acad. Sci. USA* **102,** 10451–10453 (2005).
23. Coleman, J. N. *et al.* Two-dimensional nanosheets produced by liquid exfoliation of layered materials. *Science* **331,** 568–571 (2011).
24. Mak, K. F., Lee, C., Hone, J., Shan, J. & Heinz, T. F. Atomically thin $MoS_2$: a new direct-gap semiconductor. *Phys. Rev. Lett.* **105,** 136805 (2010).
25. Splendiani, A. *et al.* Emerging photoluminescence in monolayer $MoS_2$. *Nano Lett.* **10,** 1271–1275 (2010).
26. Mak, K. F., He, K., Shan, J. & Heinz, T. F. Control of valley polarization in monolayer $MoS_2$ by optical helicity. *Nature Nanotech.* **7,** 494–498 (2012).
27. Gorbachev, R. V. *et al.* Hunting for monolayer boron nitride: optical and Raman signatures. *Small* **7,** 465–468 (2011).
28. Novoselov, K. S. Graphene: materials in the flatland. *Rev. Mod. Phys.* **83,** 837–849 (2011).
29. Dean, C. R. *et al.* Boron nitride substrates for high-quality graphene electronics. *Nature Nanotech.* **5,** 722–726 (2010).
30. Mayorov, A. S. *et al.* Micrometer-scale ballistic transport in encapsulated graphene at room temperature. *Nano Lett.* **11,** 2396–2399 (2011).
31. Ponomarenko, L. A. *et al.* Tunable metal–insulator transition in double-layer graphene heterostructures. *Nature Phys.* **7,** 958–961 (2011).
32. Furchi, M. *et al.* Microcavity-integrated graphene photodetector. *Nano Lett.* **12,** 2773–2777 (2012).
33. Engel, M. *et al.* Light–matter interaction in a microcavity-controlled graphene transistor. *Nature Commun.* **3,** 906 (2012).
34. Ferreira, A., Peres, N. M. R., Ribeiro, R. M. & Stauber, T. Graphene-based photodetector with two cavities. *Phys. Rev. B* **85,** 115438 (2012).
35. Giuliani, G. F. & Vignale, G. *Quantum Theory of the Electron Liquid* (Cambridge Univ. Press, 2005).
36. Vicarelli, L. *et al.* Graphene field-effect transistors as room-temperature terahertz detectors. *Nature Mater.* **11,** 865–871 (2012).
37. Gangadharaiah, S., Farid, A. M. & Mishchenko, E. G. Charge response function and a novel plasmon mode in graphene. *Phys. Rev. Lett.* **100,** 166802 (2008).
38. Mikhailov, S. A. & Ziegler, K. New electromagnetic mode in graphene. *Phys. Rev. Lett.* **99,** 016803 (2007).
39. Ponomarenko, L. A. *et al.* Effect of a high-kappa environment on charge carrier mobility in graphene. *Phys. Rev. Lett.* **102,** 206603 (2009).
40. Wunsch, B., Stauber, T., Sols, F. & Guinea, F. Dynamical polarization of graphene at finite doping. *N. J. Phys.* **8,** 318 (2006).
41. Hwang, E. H. & Das Sarma, S. Dielectric function, screening, and plasmons in two-dimensional graphene. *Phys. Rev. B* **75,** 205418 (2007).
42. Polini, M. *et al.* Plasmons and the spectral function of graphene. *Phys. Rev. B* **77,** 081411 (2008).
43. Abedinpour, S. H. *et al.* Drude weight, plasmon dispersion, and ac conductivity in doped graphene sheets. *Phys. Rev. B* **84,** 045429 (2011).
44. Shung, K. W. K. Dielectric function and plasmon structure of stage-1 intercalated graphite. *Phys. Rev. B* **34,** 979–993 (1986).
45. Barlas, Y., Pereg-Barnea, T., Polini, M., Asgari, R. & MacDonald, A. H. Chirality and correlations in graphene. *Phys. Rev. Lett.* **98,** 236601 (2007).
46. Reed, J. P. *et al.* The Effective Fine-Structure Constant of Freestanding Graphene Measured in Graphite. *Science* **330,** 805–808 (2010).
47. Principi, A., Polini, M. & Vignale, G. Linear response of doped graphene sheets to vector potentials. *Phys. Rev. B* **80,** 075418 (2009).
48. Ramezanali, M. R., Vazifeh, M. M., Asgari, R., Polini, M. & MacDonald, A. H. Finite-temperature screening and the specific heat of doped graphene sheets. *J. Phys. A* **42,** 214015 (2009).
49. Jablan, M., Buljan, H. & Soljacic, M. Plasmonics in graphene at infrared frequencies. *Phys. Rev. B* **80,** 245435 (2009).
50. Fei, Z. *et al.* Gate-tuning of graphene plasmons revealed by infrared nano-imaging. *Nature* **487,** 82–85 (2012).
51. Belitz, D. & Das Sarma, S. Plasmon linewidth in metals and semiconductors: a memory-function approach. *Phys. Rev. B* **34,** 8264–8269 (1986).
52. Principi, A., Asgari, R. & Polini, M. Acoustic plasmons and composite hole-acoustic plasmon satellite bands in graphene on a metal gate. *Solid State Commun.* **151,** 1627–1630 (2011).
53. Eberlein, T. *et al.* Plasmon spectroscopy of free-standing graphene films. *Phys. Rev. B* **77,** 233406 (2008).
54. Liu, Y., Willis, R. F., Emtsev, K. V. & Seyller, T. Plasmon dispersion and damping in electrically isolated two-dimensional charge sheets. *Phys. Rev. B* **78,** 201403 (2008).
55. Koch, R. J., Seyller, T. & Schaefer, J. A. Strong phonon-plasmon coupled modes in the graphene/silicon carbide heterosystem. *Phys. Rev. B* **82,** 201413 (2010).
56. Ju, L. *et al.* Graphene plasmonics for tunable terahertz metamaterials. *Nature Nanotech.* **6,** 630–634 (2011).
57. Fei, Z. *et al.* Infrared nanoscopy of Dirac plasmons at the graphene-$SiO_2$ interface. *Nano Lett.* **11,** 4701–4705 (2011).
58. Yan, H. *et al.* Tunable infrared plasmonic devices using graphene/insulator stacks. *Nature Nanotech.* **7,** 330–334 (2012).
59. Chen, J. *et al.* Optical nano-imaging of gate-tunable graphene plasmons. *Nature* **487,** 77–81 (2012).
60. Kim, J. T. & Choi, S-Y. Graphene-based plasmonic waveguides for photonic integrated circuits. *Opt. Express* **19,** 24557–24562 (2011).
61. Christensen, J., Manjavacas, A., Thongrattanasiri, S., Koppens, F. H. L. & García de Abajo, F. J. Graphene plasmon waveguiding and hybridization in individual and paired nanoribbons. *ACS Nano* **6,** 431–440 (2012).
62. Yan, H. *et al.* Infrared spectroscopy of tunable Dirac terahertz magneto-plasmons in graphene. *Nano Lett.* **12,** 3766–3771 (2012).
63. Zhou, W. *et al.* Atomically localized plasmon enhancement in monolayer graphene. *Nature Nanotech.* **7,** 161–165 (2012).
64. Crassee, I. *et al.* Intrinsic terahertz plasmons and magnetoplasmons in large scale monolayer graphene. *Nano Lett.* **12,** 2470–2474 (2012).
65. Hwang, E. H. & Das Sarma, S. Quasiparticle spectral function in doped graphene: electron-electron interaction effects in ARPES. *Phys. Rev. B* **77,** 081412 (2008).
66. Bostwick, A. *et al.* Observation of plasmarons in quasi-freestanding doped graphene. *Science* **328,** 999–1002 (2010).
67. Walter, A. L. *et al.* Effective screening and the plasmaron bands in graphene. *Phys. Rev. B* **84,** 085410 (2011).
68. Lundqvist, B. I. Single-particle spectrum of the degenerate electron gas. *Phys. Kondens. Mater.* **6,** 193–205 (1967).
69. Brar, V. W. *et al.* Observation of carrier-density-dependent many-body effects in graphene via tunneling spectroscopy. *Phys. Rev. Lett.* **104,** 036805 (2010).
70. LeBlanc, J. P. F., Hwang, J. & Carbotte, J. P. Distinguishing Coulomb and electron-phonon interactions for massless Dirac fermions. *Phys. Rev. B* **85,** 115126 (2012).
71. Peres, N. M. R. The transport properties of graphene: an introduction. *Rev. Mod. Phys.* **82,** 2673–2700 (2010).
72. Kotov, V. N., Uchoa, B., Pereira, V. M., Guinea, F. & Castro Neto, A. H. Electron-electron interactions in graphene: current status and perspectives. *Rev. Mod. Phys.* **84,** 1067–1125 (2012).
73. Barnes, W. L., Dereux, A. & Ebbesen, T. W. Surface plasmon subwavelength optics. *Nature* **424,** 824–830 (2003).
74. Maier, S. A. *Plasmonics: Fundamentals and Applications* (Springer, 2007).
75. Schedin, F. *et al.* Surface-enhanced Raman spectroscopy of graphene. *ACS Nano* **4,** 5617–5626 (2010).
76. Kravets, V. G. *et al.* Surface hydrogenation and optics of a graphene sheet transferred onto a plasmonic nanoarray. *J. Phys. Chem. C* **116,** 3882–3887 (2012).
77. Lee, J., Shim, S., Kim, B. & Shin, H. S. Surface-enhanced Raman scattering of single- and few-layer graphene by the deposition of gold nanoparticles. *Chemistry* **17,** 2381–2387 (2011).
78. Lee, J., Novoselov, K. S. & Shin, H. S. Interaction between metal and graphene: dependence on the layer number of graphene. *ACS Nano* **5,** 608–612 (2011).
79. Ling, X. *et al.* Can graphene be used as a substrate for Raman enhancement? *Nano Lett.* **10,** 553–561 (2010).
80. Ferrari, A. C. *et al.* Raman spectrum of graphene and graphene layers. *Phys. Rev. Lett.* **97,** 187401 (2006).
81. Echtermeyer, T. J. *et al.* Strong plasmonic enhancement of photovoltage in graphene. *Nature Commun.* **2,** 458 (2011).
82. Liu, Y. *et al.* Plasmon resonance enhanced multicolour photodetection by graphene. *Nature Commun.* **2,** 579 (2011).
83. Mueller, T., Xia, F. N. A. & Avouris, P. Graphene photodetectors for high-speed optical communications. *Nature Photon.* **4,** 297–301 (2010).

84. Park, J., Ahn, Y. H. & Ruiz-Vargas, C. Imaging of photocurrent generation and collection in single-layer graphene. *Nano Lett.* **9,** 1742–1746 (2009).
85. Xu, X. D., Gabor, N. M., Alden, J. S., van der Zande, A. M. & McEuen, P. L. Photo-thermoelectric effect at a graphene interface junction. *Nano Lett.* **10,** 562–566 (2010).
86. Gabor, N. M. *et al.* Hot carrier–assisted intrinsic photoresponse in graphene. *Science* **334,** 648–652 (2011).
87. Giovannetti, G. *et al.* Doping graphene with metal contacts. *Phys. Rev. Lett.* **101,** 026803 (2008).
88. Blake, P. *et al.* Influence of metal contacts and charge inhomogeneity on transport properties of graphene near the neutrality point. *Solid State Commun.* **149,** 1068–1071 (2009).
89. Kravets, V. G., Schedin, F. & Grigorenko, A. N. Fine structure constant and quantized optical transparency of plasmonic nanoarrays. *Nature Commun.* **3,** 640 (2012).
90. Atwater, H. A. & Polman, A. Plasmonics for improved photovoltaic devices. *Nature Mater.* **9,** 205–213 (2010).
91. Papasimakis, N. *et al.* Graphene in a photonic metamaterial. *Opt. Express* **18,** 8353–8359 (2010).
92. Li, X. S. *et al.* Large-area synthesis of high-quality and uniform graphene films on copper foils. *Science* **324,** 1312–1314 (2009).
93. Zou, Y., Tassin, P., Koschny, T. & Soukoulis, C. M. Interaction between graphene and metamaterials: split rings vs. wire pairs. *Opt. Express* **20,** 12198–12204 (2012).
94. Kravets, V. G. *et al.* Singular-phase nanooptics: towards label-free single molecule detection. *Nature Mater.* (submitted).
95. Kravets, V. G., Schedin, F. & Grigorenko, A. N. Extremely narrow plasmon resonances based on diffraction coupling of localized plasmons in arrays of metallic nanoparticles. *Phys. Rev. Lett.* **101,** 087403 (2008).
96. Kravets, V. G., Schedin, F., Kabashin, A. V. & Grigorenko, A. N. Sensitivity of collective plasmon modes of gold nanoresonators to local environment. *Opt. Lett.* **35,** 956–958 (2010).
97. Kabashin, A. V., Patskovsky, S. & Grigorenko, A. N. Phase and amplitude sensitivities in surface plasmon resonance bio and chemical sensing. *Opt. Express* **17,** 21191–21204 (2009).
98. Elias, D. C. *et al.* Control of graphenes properties by reversible hydrogenation: evidence for graphane. *Science* **323,** 610–613 (2009).
99. Bozhevolnyi, S. I., Volkov, V. S., Devaux, E., Laluet, J-Y. & Ebbesen, T. W. Channel plasmon subwavelength waveguide components including interferometers and ring resonators. *Nature* **440,** 508–511 (2006).

## Acknowledgements

We thank A. K. Geim, V. I. Fal'ko, M. I. Katsnelson, R. Asgari, R. Fazio, F. Guinea, A. H. MacDonald, V. Pellegrini, E. Rotenberg, F. Taddei, A. Tredicucci and G. Vignale for conversations. M.P. was supported by MIUR through the FIRB programme, grant no. RBFR10M5BT. A.N.G. was partly supported by an FP7 Metachem grant and the Samsung GRO programme.